Published in final edited form as:
Neurobiol Dis. 2012 March ; 45(3): 930–938. doi:10.1016/j.nbd.2011.12.012.

Change in the characteristics of ferritin induces iron imbalance in prion disease affected brains

Ajay Singh, **Liuting Qing**, **Qingzhong Kong**, and **Neena Singh***
Departments of Pathology and Neurology, Case Western Reserve University, 2103 Cornell Road, Cleveland, Ohio 44106.

Abstract

Prion disease associated neurotoxicity is mainly attributed to PrP-scrapie (PrP^{Sc}), the disease associated isoform of a normal protein, the prion protein (PrP^{C}). Participation of other proteins and processes is suspected, but their identity and contribution to the pathogenic process is unclear. Emerging evidence implicates imbalance of brain iron homeostasis as a significant cause of prion disease-associated neurotoxicity. The underlying cause of this change, however, remains unclear. We demonstrate that iron is sequestered in heat and SDS-stable protein complexes in sporadic-Creutzfeldt-Jakob- disease (sCJD) brains, creating a phenotype of iron deficiency. The underlying cause is change in the characteristics of ferritin, an iron storage protein that becomes aggregated, detergent-insoluble, and partitions with denatured ferritin using conventional methods of ferritin purification. A similar phenotype of iron deficiency is noted in the lumbar spinal cord (SC) tissue of scrapie infected hamsters, a site unlikely to be affected by massive neuronal death and non-specific iron deposition. As a result, the iron uptake protein transferrin (Tf) is upregulated in scrapie infected SC tissue, and increases with disease progression. A direct correlation between Tf and PrP^{Sc} suggests sequestration of iron in dysfunctional ferritin that either co-aggregates with PrP^{Sc} or is rendered dysfunctional by PrP^{Sc} through an indirect process. Surprisingly, amplification of PrP^{Sc} *in vitro* by the protein-misfolding-cyclic-amplification (PMCA) reaction using normal brain homogenate as substrate does not increase the heat and SDS-stable pool of iron even though both PrP^{Sc} and ferritin aggregate by this procedure. These observations highlight important differences between PrP^{Sc}-protein complexes generated *in vivo* during disease progression and *in vitro* by the PMCA reaction, and the significance of these complexes in PrP^{Sc}-associated neurotoxicity.

Keywords

Prion disorders; ferritin; PrP-scrapie; brain iron imbalance; aggregation; neurotoxicity

Introduction

Sporadic Creutzfeldt-Jakob disease (sCJD) is a progressive, fatal neurodegenerative condition of humans that is included in the general category of prion disorders. Unlike most

*Address correspondence to Neena Singh, neena.singh@case.edu.

Author disclosure statement
No competing financial interests exist for AS, LQ, QK, and NS.

neurodegenerative conditions, prion disorders are transmissible in addition to their sporadic and familial nature, a characteristic that has raised significant public health concern. sCJD is the most common human prion disorder, comprising ~80% of all diagnosed cases. The infectious and pathogenic agent in all prion disorders is believed to be PrP-scrapie (PrP^{Sc}), a β-sheet rich isoform of a normal protein, the prion protein (PrP^{C}). The conformational switch from PrP^{C} to PrP^{Sc} is triggered by exogenous PrP^{Sc} in transmissible disorders, mutation in the prion protein gene in familial cases, and by a random event in sporadic disorders. Unlike PrP^{C} that is mainly α-helical, soluble in non-ionic detergents and sensitive to proteases, PrP^{Sc} requires harsh conditions such as sodium dodecyl sulfate (SDS) or guanidinium hydrochloride treatment for complete solubilization, and is resistant to limited digestion by proteinase K (PK) (Prusiner 1998; Aguzzi and Callela, 2009; Caughey et al., 2009; Soto and Satani, 2010). The recent amplification of PrP^{Sc} from recombinant PrP^{C} *in vitro* by the protein misfolding cyclic amplification reaction (PMCA) leaves little doubt that PrP^{Sc} arises from PrP^{C}, and is sufficient to transmit the disease in bioassays (Deleault et al., 2007; Wang et al., 2010). The mechanism by which PrP^{Sc} induces neurotoxicity, however, is less clear. Existing evidence suggests expression of host-encoded PrP^{C} on neuronal plasma membrane as an essential component of the toxic signal (Chesebro et al 2005; Mallucci et al., 2007; Radford and Mallucci, 2007). Contribution of other proteins and molecules, though speculated, has remained elusive (Resenberger et al., 2011).

Recent reports indicating mis-regulation of iron metabolism in sCJD and scrapie infected animal brains implicate redox-iron in prion disease pathogenesis, an important observation given the highly toxic nature of unliganded iron and its documented involvement in other neurodegenerative conditions of protein misfolding such as Alzheimer's disease (AD), Parkinson's disease, and Huntington's disease (Singh et al, 2009a, 2010, 2011; Bonda et al. 2011; Kell, 2009, 2010; Das et al., 2010; Smith et al., 2010; Lee and Andersen 2010; Altamura and Muckenthaler, 2009; Madsen and Gitlin, 2007; Molina-Holgado et al., 2007; Kim et al., 2007; Berg and Youdim, 2006; Adlard and Bush 2006). The diverse etiology and pathogenesis of these disorders has led to the general notion that brain iron dyshomeostasis is an epiphenomenon of massive neuronal death associated with these conditions. However, mounting evidence suggests that the change in brain iron precedes neuronal degeneration, and is often the main trigger for neurotoxicity. Specific examples include inherited disorders of brain iron imbalance such as neurodegeneration with brain iron accumulation, neuroferritinopathy, infantile neuroaxonal dystrophy-1, aceruloplasminemia, Friedreich's ataxia, and Restless Leg Syndrome (RLS) (Johnstone and Milward, 2010). A similar association between iron imbalance and neurotoxicity is less clear for sporadic disorders. However, a recent study demonstrating inhibition of ferroxidase activity of Alzheimer precursor protein (APP) as the underlying cause of iron accumulation in AD brains has re-kindled this debate (Duce et al., 2010), necessitating reevaluation of the mechanism and significance of brain iron imbalance in other neurodegenerative conditions of sporadic origin.

At variance with AD, sCJD brains reveal a phenotype of 'apparent' iron deficiency as indicated by upregulation of the iron uptake protein transferrin (Tf) despite minimal change in total brain iron (Singh et al., 2009a). Tf levels increase with disease progression and correlate with PrP^{Sc} levels, indicating a close association with the underlying disease process. An unexpected change in Tf levels is also noted in the cerebrospinal fluid (CSF) of sCJD cases, suggesting mis-regulation of iron homeostasis in cells of the blood-brain and brain-CSF barriers in addition to brain parenchymal cells (Singh et al., 2011). Mis-regulation of iron homeostasis has also been reported in PrP^{Sc} replicating cells lines, mouse and hamster models of prion disease, and familial cases associated with PrP102L mutation, demonstrating the generality of this phenomenon across species and experimental models (Fernaeus et al., 2005; Fernaeus and Land, 2005; Petersen et al., 2005; Hur et al., 2002; Kim

et al., 2007, Singh et al., 2009). A systems biology approach to this question reveals a similar association between brain iron mis-metabolism and prion disorders, reinforcing the significance of this phenomenon in prion disease pathogenesis (Hwang et al., 2009; Kell, 2009). The underlying cause of this change has been difficult to understand due to the complex nature of brain iron homeostasis compounded further by disease pathogenesis. Possible mechanisms include loss of normal function of PrP^{C} in iron uptake and transport, and/or disruption of brain iron metabolism by PrP^{Sc} directly or indirectly (Singh et al., 2009a–c). In this regard, it is interesting to note that PrP^{Sc} co-purifies with ferritin, a major iron storage protein using different experimental procedures (Saunders et al., 2007). Although considered an artifact of experimental manipulation (Moore et al., 2010), PrP^{Sc} and ferritin have been demonstrated to co-localize in the lysosomes of scrapie infected cell lines, suggesting *in vivo* interaction and possible co-aggregation at that site (Singh et al., 2009). Sequestration of iron in such PrP^{Sc}-ferritin aggregates is likely to induce iron deficiency, resulting in the observed brain iron dyshomeostasis.

To evaluate whether sequestration of iron in PrP^{Sc}-ferritin complexes generated during disease progression is the underlying cause of iron deficiency in prion disease affected brains, the stability of iron in protein complexes precipitated from sCJD brain homogenates was compared with age-matched dementia controls and with PrP^{Sc}-protein complexes generated *in vitro* by the PMCA reaction using normal brain homogenate as substrate. We report that iron is sequestered in heat and SDS-stable protein complexes in sCJD brain homogenates, a characteristic that is specific to sCJD among the dementia cases included in this study. In contrast, precipitated proteins from the PMCA reaction mix release associated iron readily under similar conditions even though comparable amounts of aggregated and PK-resistant ferritin and PrP^{Sc} are generated by this procedure. These observations highlight important differences between PrP^{Sc}-protein complexes generated *in vivo* and *in vitro*, and underscore the significance of PrP^{Sc}-associated proteins in the pathogenesis of sCJD.

Methods

Materials and antibodies

Antibodies to PrP (3F4) and GFAP were obtained from Abcam (Cambridge, MA, USA), and anti-PrP antibody 8H4 was a kind gift from Man-Sun Sy (Case Western Reserve University). Antibodies to other antigens were procured as follows: ferritin from Sigma (Saint Louis, MO, USA), Tf from GeneTex (San Antonio, TX, USA), actin from Millipore (Temecula, CA, USA), and ceruloplasmin from Dako (A/S Denmark). Horseradish peroxidase (HRP)-conjugated secondary antibodies were purchased from GE Healthcare (Little Chalfont, Buckinghamshire, UK). Iron estimation kit was procured from Stanbio Laboratory (Boerne, TX, USA), and $^{59}FeCl_3$ was obtained from Perkin Elmer (Boston, MA, USA). All other chemicals were purchased from Sigma.

Human and animal samples

Autopsy confirmed frozen human brain tissue from the frontal cortex of sCJD (CJD+, n=20) and age matched cases of dementia (CJD−, n=19) were obtained from the National Prion Disease Pathology Surveillance Center at Case Western Reserve University. The samples ranged in age from 37–80 years, with most in the 60–80 year range. The interval between appearance of clinical symptoms and death ranged from 1–24 months in CJD− and 2 to 4 months in CJD+ cases. CJD− cases included extensive infarcts, granulomatous angiitis, cerebral vascular disease, and necrotizing lymphoplasmacytic meningoencephalitis (1 case each), Alzheimer's disease (6 cases), and no definitive diagnosis (9 cases). CJD+ cases were classified as MM1 (11 cases), VV1 (2 cases), VV2 (4 cases), and MV2 (3 cases). Control and prion infected hamster spinal cord samples were obtained from Jason Bartz (Department

of Medical Microbiology and Immunology, Creighton University, Omaha, Nebraska), and represented tissue from L4 and L6 lumbar spinal cord segments harvested at 28, 42, 55, and 70 days post inoculation (Bartz et al., 2007). Control mouse brain and liver was harvested from 3–5 month old FVB/NJ mice (Jackson Laboratory) housed at Case Western Reserve University. ^{59}Fe-labeled brain liver samples for PMCA reactions were generated by injecting 20μCi of $^{59}FeCl_3$ to FVB/NJ mice via tail vein followed by a chase for 24h. Mice were euthanized, perfused with cold PBS, and relevant organs were harvested. All tissue was snap frozen and stored at −80°C until use. Tissue homogenates (10%) were prepared either in lysis buffer (10 mM Tris, pH 7.5, 150 mM NaCl, 0.5% sodium deoxycholate, 0.5% NP-40, and protease inhibitor cocktail), or PMCA buffer (phosphate buffered saline, pH 7.2–7.4, 0.15M NaCl, 1% Triton X-100, 4mM EDTA and protease inhibitor cocktail) (Castilla et al., 2005).

Iron estimation

For determination of iron in heat and SDS insoluble complexes in CJD− and CJD+ cases, homogenates prepared in lysis buffer were supplemented with SDS to a final concentration of 1% and either kept at room temperature or heated at 100°C for 10 min. Samples were cooled to room temperature, vortexed vigorously, and precipitated with five volumes of cold methanol followed by centrifugation at 20,000 × g for 15 min. Likewise, samples from spinal cord of tissue of scrapie infected hamsters and −/+PMCA reactions were precipitated with cold methanol and centrifuged as above. Iron in protein pellets was quantified as described by Rebouche et al. (2004) with modifications. Samples were mixed with equal volume of 1 N HCl and 10% trichloroacetic acid, vortexed, and heated at 95°C for 1h. Contents were cooled to room temperature, vortexed, and centrifuged at 12,000 × g for 20 min at 20°C. Iron in the supernatant was quantified by the Stanbio iron estimation kit as per manufacturer's instructions.

Differential centrifugation

To partition proteins in CJD− and CJD+ samples into detergent soluble and insoluble fractions, homogenates prepared in lysis buffer were supplemented with SDS to 1% final concentration and subjected to differential centrifugation. Samples in duplicate were initially centrifuged at low speed (3,000 rpm) for 1 min to obtain low speed pellet (P1) and supernatant (S1) fractions. One set of S1 and P1 samples was kept aside and the second S1 fraction was centrifuged at 20,000 × g for 3h to obtain high speed pellet (P2) and supernatant (S2) fractions. The P1 and P2 fractions were reconstituted to original volume with lysis buffer. All fractions were boiled with sample buffer and fractionated by SDS-PAGE followed by Western blotting. A parallel set of samples were precipitated with cold methanol and iron in the pellet was quantified as described above.

For partitioning of proteins from the PMCA reaction mix, −/+PMCA samples in PMCA buffer were centrifuged at 20,000 × g for 3 h to obtain soluble (S) and insoluble pellet (P) fractions. Where indicated, samples were treated with 50 or 100μg/ml of proteinase K at 37°C for 1h. Reaction was stopped by boiling in 5× SDS sample buffer.

Fractionation of soluble and insoluble ferritin

Normal and scrapie infected mouse brain homogenates (10%) were prepared in PBS and heated at 75°C for 10 min as described (Harrison and Arosio 1996; Koorts and Viloen, 2007). Samples were vortexed and centrifuged at 10,000 × g for 15 min to obtain soluble (supernatant) and insoluble (pellet) ferritin fractions. Pellets were dissolved in equivalent volume of PBS, boiled with 5× SDS sample buffer, and subjected to Western blotting.

PMCA and treatment with proteinase-K

PMCA reaction was carried out as described by Castilla et al. (2005) with modifications. In short, 10% homogenates of perfused liver or brain tissue prepared in PMCA buffer were clarified at 1500g for 30 sec. Samples were aliquoted in 0.2 ml PCR tubes and stored at −80°C till further use. PMCA reaction was carried out in a programmable sonicator (Misonix, USA, Model S3000MP) with a sonication pulse of 40 sec “ON” and 10 min “OFF” at an amplitude of 60 for 24h. Reaction tubes were immersed in sonicator water bath set at 40°C without shaking. Control (−PMCA) samples were kept at −80°C till completion of reaction. Where indicated, mouse or hamster scrapie seed was used at a dilution of 1:100. PMCA of ^{59}Fe-labeled brain and liver homogenates was carried out as above.

SDS-PAGE and Western blotting

Samples were mixed with Lamelli SDS-PAGE sample buffer, heated at 95°C for 5 min, and resolved by SDS-PAGE followed by electrotransfer to PVDF membranes. Membranes containing transferred proteins were immunoreacted with the following antibodies sequentially: PrP (3F4 or 8H4 for hamster and mouse tissue respectively), ferritin (1:1000), Tf (1:6000), GFAP (1:2000), ceruloplasmin (1:2500) and β-actin (1:7500), followed by anti-mouse or anti-rabbit secondary antibody conjugated to horseradish peroxidase (1:6000). Immunoreactive bands were visualized by the ECL detection kit (Amersham Biosciences Inc.).

Statistical analysis

Most experiments were performed in triplicate and all experiments were repeated at least three times. The results are expressed as mean ± standard error of mean (SEM). Statistical analysis was done by unpaired Student's t-test for comparing two groups. Comparison of multiple groups was done by one way ANOVA followed by Bonferroni multiple comparison post hoc test using GraphPad Prism software (Version 4.03, GraphPad Inc., San Diego, CA, USA). Regression analysis was performed by standard statistical methods and the Stata (2005) statistical package. Differences were considered significant at $p<0.05$.

Results

Iron is sequestered in heat and SDS-stable protein complexes in sCJD brain homogenates

To understand the cause of progressive iron deficiency in sCJD and scrapie infected hamster brains despite minimal change in total iron (Singh et al., 2009a), possible sequestration of iron in aggregated PrP^{Sc}-protein complexes was explored. Tissue from the frontal cortex of sCJD (CJD+) and age-matched non-CJD dementia controls (CJD−) was homogenized in a buffer containing non-ionic detergents (lysis buffer) supplemented with 1% SDS, and either set aside at room temperature or boiled for 10 minutes. Since most iron binding proteins release associated iron after boiling (Harrison and Arosio 1996; Koorts and Viloen, 2007), iron content of methanol precipitated proteins from unboiled and boiled samples was quantified. Unboiled CJD− and CJD+ samples revealed similar iron content. However, boiled CJD− samples released 68% of associated iron while CJD+ samples lost minimal iron relative to unboiled controls (Figure 1 A). A direct comparison of boiled samples revealed 183% more iron in CJD+ relative to CJD− samples (Figure 1 A). Comparison with Alzheimer’s disease (AD) brains that are known to accumulate iron revealed similar results (Figure 1 B), suggesting that the heat and SDS stable pool of iron is specific to sCJD brains (Duce et al., 2010).

Among the iron rich proteins likely to contribute to the heat stable pool of iron, ferritin stands out since it is known to co-purify with PrP^{Sc} and resists denaturation at 75–80°C, a property often exploited to enrich tissue fractions for iron rich ferritin (Moore et al., 2010;

Harrison and Arosio 1996; Koorts and Viloen, 2007). To evaluate a possible change in the characteristics of ferritin due to a direct or indirect interaction with PrP^{Sc}, brain samples prepared as above were centrifuged at low speed to separate detergent soluble proteins (S1) from insoluble debris in the pellet (P1), and soluble proteins in the S1 fraction were re-centrifuged at high speed to isolate detergent soluble (S2) and insoluble (P2) proteins. Pellets were re-dissolved in lysis buffer and all samples were subjected to SDS-PAGE and Western blotting. As expected, almost all of PrP^{C} from CJD− samples partitioned in detergent soluble S1 and S2 fractions (Figure 1 C, lanes 1 & 3). Minimal reactivity for PrP was detected in P1 and almost no reactivity in the P2 fraction (Figure 1 C, lanes 2 & 4). In contrast, a significant amount of PrP^{Sc} from CJD+ samples fractionated in the low and high speed pellet fractions (P1 and P2) (Figure 1C, lanes 6 & 8). The shift of PrP^{Sc} from high speed detergent soluble S2 to the detergent insoluble P2 fraction was most dramatic relative to controls (Figure 1 C, lanes 7 & 8, *). Re-probing for ferritin revealed most of the reactivity in S1 and S2 fractions of CJD− cases (Figure 1 C, lanes 1 & 3), and a significant shift from S2 to the P2 fraction of CJD+ cases as observed for PrP^{Sc} (Figure 1 C, lanes 7 & 8, arrow-head). Transferrin (Tf), a major iron uptake protein, and ceruloplasmin (Cp), a copper containing ferroxidase, partitioned in the detergent soluble S1 and S2 fractions in both CJD− and CJD+ cases, indicating selective partitioning of ferritin in the P2 fraction of CJD+ samples among the three iron management proteins tested (Figure 1 C, lanes 1, 3, 5, & 7). Re-probing for β-actin revealed similar protein loading in S1 and S2 fractions of CJD− and CJD+ samples (Figure 1 C, lanes 1, 3, 5, & 7). (Partitioning of β-actin in P1 and P2 fractions varies with detergent composition and centrifugation speed, and is therefore unreliable (unpublished observations).

Quantification by densitometry revealed 182% more PrP in the S1 fraction of CJD+ relative to CJD− samples as expected. Ferritin levels were similar in the two groups (Figure 1 D). Estimation of iron in methanol precipitated proteins from soluble and insoluble fractions of CJD+ samples revealed almost complete correspondence with ferritin, indicating that the major iron containing protein in the brain tissue is ferritin, and aggregated ferritin in CJD+ samples is loaded with iron (Figure 1 E).

To rule out artifactual co-sedimentation of ferritin with PrP^{Sc} (Moore et al., 2010), ferritin was fractionated in PBS or water, conditions normally used for the enrichment of tissue ferritin. Under these condition, ferritin partitions in the soluble phase, while denatured ferritin and hemosiderin sediment as insoluble proteins (Kontoghiorghes et al., 1987; Harrison and Arosio 1996). PrP^{C} and PrP^{Sc}, being membrane proteins, are likely to remain attached to the lipid bilayer in the absence of detergent and sediment in chunks of membrane or in lipid micelles. Thus, soluble ferritin and PrP^{C} or PrP^{Sc} are unlikely to interact and co-aggregate non-specifically under these conditions. To compare the solubility of ferritin from normal and diseased brains, whole brains from scrapie infected mice (MSc) and matched controls (NH) were homogenized in PBS and heated at 75°C for 10 minutes, a treatment that spares ferritin but denatures most other proteins. After vigorous vortexing, samples were centrifuged to pellet denatured proteins, and soluble and insoluble fractions were boiled in sample buffer and analyzed (Figure 2 A). Probing for ferritin showed insignificant difference between soluble and insoluble fractions of NH samples, and a significant shift to the insoluble fraction in MSc samples (Figure 2 A, lanes 1–5 vs. 10–14 & lanes 6–9 vs. 15–18 respectively). Re-probing for PrP revealed most of the reactivity in the insoluble fraction as expected (Figure 2 A, lanes 10–18). Minimal or no reactivity for PrP was detected in the soluble fraction (Figure 2 A, lanes 1–9). Actin partitioned mainly in the insoluble fraction under these conditions (Figure 2 A, lanes 1–18).

Quantification revealed 4.0 fold more ferritin in the insoluble fraction of MSc samples relative to only 0.9 fold increase in NH samples (Figure 2 B), indicating that a significant amount of ferritin in scrapie infected brains is denatured.

Together, the above results suggest that the increase in heat and SDS stable iron in CJD+ brains is probably due to sequestration of iron in aggregated, dysfunctional ferritin subunits.

Iron deficiency increases with disease progression in the lumbar spinal cord of scrapie infected hamsters

To evaluate whether sequestration of iron in dysfunctional ferritin influences iron homeostasis in diseased tissue, expression of Tf, a major iron uptake protein, and iron content were monitored in scrapie infected samples during disease progression. To avoid artifacts due to hemosiderin deposits from massive neuronal death in the brain and possible leakage from the blood brain barrier (BBB), lumbar spinal cord tissue of hamsters inoculated with scrapie in the sciatic nerve was evaluated (Bartz et al., 2007; Goodbrand et al., 1995; Iwasaki et al., 2005). Samples harvested at 28, 42, 55, and 70 days post-inoculation (pi) were homogenized in lysis buffer and analyzed by SDS-PAGE and Western blotting. Membranes were probed for PrP to track accumulation of PrP^{Sc}, and for Tf and ferritin to detect change(s) in intracellular labile iron pool (LIP). Tf is normally up regulated and ferritin down regulated during iron deficiency to replenish depleted LIP, and the opposite scenario takes effect under conditions of iron excess (Rouault and Cooperman, 2006). Expression of glial fibrillary acidic protein (GFAP) was checked to estimate astrogliosis during disease progression. As expected, levels of PrP showed a significant increase after 55 days pi and continued to increase till 70 days (Figure 3, lanes 1–11). Surprisingly, Tf levels showed a similar pattern of increase, rising significantly at 55 and 70 days pi relative to the 28 day sample (Figure 3, lanes 1–11). The increase was more significant in brain specific β2 form of Tf, ruling out any artifacts due to leakage from the BBB (Irjala et al., 1979; Meurman et al., 1979). Levels of ferritin did not change significantly during the disease course although GFAP levels increased after 55 days and continued to rise till 70 days pi (Figure 3, lanes 1–11). Re-probing for β-actin confirmed that the observed differences were not an artifact of protein loading (Figure 3, lanes 1–11).

Quantification by densitometry revealed that the increase in PrP, Tf, and GFAP expression was significant at 55 and 70 days pi relative to the 28 day time point, while ferritin did not show a significant change at any time point. PrP increased by 66% and 127%, GFAP by 117% and 193%, and Tf by 110% and 385% after 55 and 70 days relative to 28 days pi respectively (Figure 4 A). Total iron showed a modest increase of 26.6% after 70 days relative to 28 days pi (Figures 4 B). Regression plot of Tf and PrP during disease progression showed a strong correlation (R^2=.801, 95% confidence interval (CI)), indicating that Tf increases as PrP^{Sc} accumulates (Figure 4 C).

These results indicate that iron deficiency becomes apparent in scrapie infected spinal cord tissue at 55 days pi, and continues to increase till end stage of disease despite minimal change in brain iron levels. More importantly, a positive correlation between Tf and PrP^{Sc} suggests that iron deficiency increases as PrP^{Sc} accumulates.

Amplification of PrP^{Sc} *in vitro* does not alter the heat and SDS stable pool of iron

To evaluate whether insolubility of ferritin is due to direct interaction with PrP^{Sc}, brain homogenate from wild type mice was used as substrate to amplify PrP^{Sc} *in vitro* by the PMCA reaction (Castilla et al., 2005). This procedure replicates PrP^{Sc} several thousand-fold by converting normal PrP^{C} to PrP^{Sc}, mimicking prion propagation *in vivo*. Two experimental paradigms were attempted: 1) mouse PrP^{Sc} was amplified using ME7 strain of

mouse scrapie as seed and normal mouse brain as substrate, and 2) hamster PrP^{Sc} was amplified using hamster scrapie as seed and a 1:1 mixture of hamster brain and mouse liver as substrate. Addition of mouse liver in the second experimental paradigm provided a source of L-ferritin from a heterologous species, providing an opportunity to determine whether the interaction with PrP^{Sc} is specific to H-chain rich brain ferritin from a homologous species, and whether PrP^{Sc} seeds the aggregation of ferritin and vice-versa.

Brain homogenates from FVB wild-type mice prepared in PMCA buffer (Castilla et al., 2005) were seeded with mouse scrapie and set aside (−PMCA), or subjected to PMCA for 24 hours (+PMCA). Half of each sample was treated with 50μg/ml of proteinase-K (PK) or buffer for 1 hour at 37°C and analyzed by Western blotting. Probing for PrP revealed complete degradation in −PMCA samples (Figure 5 A, lanes 2 and 6), while +PMCA samples showed a significant amount of PK-resistant PrP^{Sc} (Figure 5 A, lanes 4 and 8). Re-probing for ferritin showed a surprisingly similar pattern; ferritin was completely degraded by PK in −PMCA samples (Figure 5 A, lanes 2 and 6), whereas +PMCA samples revealed prominent PK-resistant H- and L-forms of ferritin, of which the L-form appeared more resistant (Figure 5 A, lanes 4 and 8, arrow-head). In addition, a partially digested, faster migrating band of ferritin appeared after PK-digestion (Figure 5 A, lanes 4 and 8). It is difficult to assess whether this fragment arose from H- or L-chain ferritin because their ratio changes after PMCA, and both forms decrease in intensity after PK (Figure 5 A, compare lane 1 with 3 & 4, and lane 5 with 7 & 8). Ponceu-S staining of the PVDF membrane revealed degradation of most proteins by PK in −PMCA samples (Figure 5 B, lanes 2 and 6, *), and several PK-resistant bands in +PK samples despite an overall decrease in total proteins due to sonication (Figure 5 B, compare lanes 1 & 5 with 4 & 8, arrow-head).

A similar reaction was performed using a mixture of hamster brain and mouse liver (1:1) as substrate and hamster scrapie as seed. Treatment with 50μg/ml of PK resulted in almost complete degradation of PrP and ferritin in −PMCA samples (Figure 5 C, lanes 2, 6, & 10), and gave rise to typical PK-resistant forms of PrP^{Sc} and a PK-resistant ferritin band in +PMCA samples (Figure 5 C, lanes 4, 8, & 12). In contrast to mouse brain ferritin, liver ferritin required twice the amount of PK to generate the 15kDa degradation product of ferritin (Figure 5 C, lanes 4, 8, & 12).

Surprisingly, the heat stable pool of iron did not change significantly in PMCA products from scrapie seeded mouse and hamster brain homogenates even though significant amounts of aggregated and PK-resistant PrP^{Sc} and ferritin were generated (Figure 5 D). Similar results were obtained when ^{59}Fe-labeled mouse brain homogenates were seeded with mouse PrP^{Sc} in a PMCA reaction to increase the sensitivity of detection (data not shown).

It was surprising that brain and liver ferritin acquired PK-resistance following PMCA. To evaluate whether ferritin aggregates regardless of PrP^{Sc}, liver tissue that expresses minimal amounts of PrP^{C} was subjected to PMCA without added PrP^{Sc} seed. An aliquot from each reaction mix was set aside to control for total protein (T). The rest was centrifuged to separate soluble (S) and aggregated pellet (P) fractions. All samples were analyzed by Western blotting. Probing of T samples for ferritin, Tf, and Cp showed similar protein levels in −PMCA and +PMCA samples, indicating minimal degradation of these proteins by PMCA (Figure 6 A, lanes 1–6). After centrifugation, ferritin partitioned equally between S and P fractions in −PMCA samples, and shifted completely to the P fraction in +PMCA samples (Figure 6 A, lanes 7–18, *). In contrast, Tf and Cp partitioned exclusively in the S fraction in both −PMCA and +PMCA samples (Figure 6 A, lanes 7, 9, 11, 13, 15, & 17). As observed in Figure 5 B above, Ponceu-S stained proteins showed an overall decrease in +PMCA samples relative to −PMCA controls (Figure 6 A, lanes 1–18), and aggregation of several proteins following PMCA (Figure 6 A, lanes 10, 14, and 18, *).

Quantification of ferritin and protein associated iron in S and P fractions of −PMCA and +PMCA samples revealed almost equal distribution in the former, and a shift to the P fraction in the latter. Distribution of ferritin in the S and P fractions of −PMCA samples was 56.6% and 43.4%, and of iron 53.1% and 46.9%. In +PMCA samples the distribution of ferritin in S and P fractions was 2.5% and 97.5%, and that of iron 30% and 70% respectively (Figure 6 B C). Thus, aggregated ferritin in the P fraction of +PMCA samples is loaded with iron. The presence of relatively more iron relative to ferritin in the S fraction of +PMCA samples indicates contribution from Tf and perhaps other iron associated proteins that do not aggregate by PMCA. A similar evaluation of ^{59}Fe-radiolabeled liver samples revealed shift of ^{59}Fe counts to the P fraction following PMCA, confirming the above results (data not shown).

Together, these results indicate that *in vitro* generation of potentially infectious and PK-resistant PrP^{Sc} or aggregated and PK-resistant ferritin in brain homogenates by the PMCA reaction either singly or in combination are insufficient to render associated iron resistant to heat and SDS.

Discussion

We demonstrate that a significant amount of iron in sCJD brain homogenates is associated with protein complexes in a heat and SDS-stable form, creating brain iron bio-insufficiency and a phenotype of iron deficiency that increases with disease progression. The underlying cause is change in the characteristics of brain ferritin that becomes insoluble in detergents, co-sediments with PrP^{Sc}, and partitions with dysfunctional ferritin or hemosiderin in the presence of PBS or water (Kontoghiorghes et al., 1987; Harrison and Arosio 1996). Upregulation of Tf in diseased brain and spinal cord tissue suggests that dysfunctional ferritin accumulates in an intracellular compartment in viable cells that respond appropriately to the functional iron deficiency (Singh et al., 2009a). A direct correlation between Tf and PrP^{Sc} suggests co-aggregation of ferritin with PrP^{Sc} or an indirect influence of PrP^{Sc} on ferritin function. However, amplification of infectious PrP^{Sc} *in vitro* by the PMCA reaction using normal brain homogenate as substrate does not increase the heat and SDS stable pool of iron although comparable amounts of aggregated and PK-resistant PrP^{Sc} and ferritin are generated by this method. These data suggest that *in vivo* interaction of PrP^{Sc} with ferritin or other iron modulating protein(s) induces brain iron deficiency, highlighting important differences between potentially infectious PrP^{Sc} generated *in vitro* by the PMCA reaction and pathogenic PrP^{Sc}-protein complexes in diseased brains that are likely to play a significant role in delivering the toxic signal of PrP^{Sc}.

The presence of heat and SDS-stable protein-associated pool of iron in sCJD brains is unexpected, and contrasts with other dementias associated with iron accumulation. This is surprising since the course of sCJD is rapid relative to other dementias, giving little opportunity for iron to accumulate in insoluble hemosiderin deposits. Moreover, unlike several other dementias where hemosiderin collects in a relatively inactive form in the extracellular milieu and does not influence the expression of iron management proteins, sCJD brain and scrapie infected hamster spinal cord tissue shows upregulation of Tf without a significant decrease in brain iron levels, indicating intracellular accumulation of bio-unavailable iron. AD brains also accumulate iron due to the compromised ferroxidase activity of APP, but unlike sCJD, cells are able to sense accumulated iron and respond appropriately by down-regulating iron uptake proteins Tf and TfR and upregulating the iron storage protein ferritin (Duce et al., 2010). Furthermore, iron from AD brain homogenates is released readily by boiling in the presence of SDS, indicating a distinct mechanism of accumulation. The unusual resilience of protein-associated iron in sCJD brains could be attributed to dysfunctional ferritin as a result of direct or indirect interaction with PrP^{Sc}, or

co-precipitation of iron released from dead cells with PrP^{Sc} aggregates (Prusiner, 1998). Since Tf is upregulated in diseased brains, the latter possibility is less likely. The absence of heat and SDS-stable pool of iron in the PMCA reaction mix despite the presence of aggregated PrP^{Sc} and ferritin further suggests that *in vivo* interaction of these proteins is responsible for sequestering iron in stable protein aggregates, not non-specific co-aggregation due to the sticky nature of PrP^{Sc} (Moore et al., 2010). Co-localization of PrP^{Sc} and ferritin in the lysosomes of scrapie infected cell lines and increase in the autophagosomal marker LC3 II in sCJD and scrapie infected hamster brains suggests possible co-aggregation at this locale, a site where both PrP^{Sc} and ferritin turnover (Singh et al., 2009a; Das et al., 2010; Heiseke et al., 2010).

Surprisingly, PMCA induces aggregation and PK resistance of ferritin regardless of its heavy and light chain ratio or the presence of PrP^{Sc} in the reaction mix. Aggregated ferritin thus generated is loaded with iron that is released readily by boiling. Several other proteins also aggregate and acquire PK resistance following PMCA, a property that depends on the aggregation state of a specific protein under the buffer conditions used and the intensity of sonication (unpublished observations). However, unlike PrP^{C} that needs homologous PrP^{Sc} seed for aggregation and replication, ferritin undergoes aggregation without seed after one cycle and does not catalyze the aggregation of additional ferritin under the conditions used for the amplification of PrP^{Sc} (unpublished observations). Other iron management proteins such as Tf, TfR, and Cp do not aggregate following PMCA or in sCJD brain homogenates, suggesting that ferritin is probably the only iron rich protein that is prone to aggregation.

Whether co-aggregation of ferritin with PrP^{Sc} is the sole cause of iron deficiency in sCJD brains cannot be concluded unequivocally from our data. It is likely that ferritin becomes dysfunctional by disease specific processes that are related indirectly to PrP^{Sc} accumulation. Other possibilities include loss of normal function of PrP^{C} in iron uptake due to aggregation to the PrP^{Sc} form (Singh et al., 2009b), functional impairment of copper containing ferroxidases due to sequestration of PrP^{C}-associated Cu ions within PrP^{Sc} (Singh et al., 2010), or co-aggregation of other proteins involved directly or indirectly in maintaining brain iron homeostasis. Although not mutually exclusive, our observations favor co-aggregation of PrP^{Sc} with ferritin as the most likely possibility. Stabilization of PrP^{Sc} by iron and a strong affinity of PrP^{Sc} for iron oxide support this assumption (Basu et al., 2007; Miller and Supattapone, 2011). Relative stabilization and acquisition of PK-resistance by PrP^{C} has also been reported due to interaction with manganese (Mn), another divalent cation implicated in the pathogenesis of prion disorders (Hesketh et al., 2008; Choi et al., 2010). Moreover, levels of divalent metal transporter (DMT1) and Tf are altered in scrapie infected cell lines, suggesting mis-metabolism of several other metals besides iron during prion disease pathogenesis (Choi et al., 2006, 2007; Martin et al., 2011).

In conclusion, our data underscore the significance of PrP^{Sc}-protein complexes formed during disease progression *in vivo*, and suggest that the nature of the toxic signal by PrP^{Sc} is likely to be determined by the associated proteins rather than PrP^{Sc} *per se*, an area that requires further investigation.

Highlights

- Iron is trapped in heat and SDS-stable protein complexes in sCJD brains
- This causes iron deficiency that correlates with PrP^{Sc}
- Iron may be trapped in PrP^{Sc}-ferritin complexes in an intracellular compartment
- PrP^{Sc} and ferritin do not co-aggregate in a PMCA reaction

- PrP^{Sc}-protein complexes formed *in vivo* differ from PrP^{Sc} generated by PMCA

Abbreviations

PrP^{Sc}	PrP-scrapie
PrP^{C}	normal cellular PrP
Tf	transferrin
Cp	ceruloplasmin

Acknowledgments

Special thanks are extended to Dr. Jason Bartz (Creighton University, Omaha, Nebraska) for providing scrapie infected hamster spinal cord tissue, and to the National Prion disease Surveillance Center for providing brain tissue from sCJD cases. This study was supported by grants R21AG033423 and R01DK088390 (to NS) from the National Institutes of Health.

References

Adlard PA, Bush AI. Metals and Alzheimer's disease. J Alzheimers Dis. 2006; 10:145–163. [PubMed: 17119284]

Aguzzi A, Calella AM. Prions: protein aggregation and infectious diseases. Physiol Rev. 2009; 89:1105–1152. [PubMed: 19789378]

Altamura S, Muckenthaler MU. Iron toxicity in diseases of aging: Alzheimer's disease, Parkinson's disease and atherosclerosis. J Alzheimers Dis. 2009; 16:879–895. [PubMed: 19387120]

Bartz JC, Kramer ML, Sheehan MH, Hutter JAL, Ayers JI, Bessen RA, Kincaid AE. Prion Interference Is Due to a Reduction in Strain-Specific PrP^{Sc} Levels. J Virol. 2007; 81:689–697. [PubMed: 17079313]

Basu S, Mohan ML, Luo X, Kundu B, Kong Q, Singh N. Modulation of PK-resistant PrP^{Sc} in cells and infectious brain homogenate by redox-iron: Implications for prion replication and disease pathogenesis. Mol Biol Cell. 2007; 18:3302–3312. [PubMed: 17567949]

Berg D, Youdim MB. Role of iron in neurodegenerative disorders. Top Magn Reson Imaging. 2006; 17:5–17. [PubMed: 17179893]

Bonda DJ, Lee HG, Blair JA, Zhu X, Perry G, Smith MA. Role of metal dyshomeostasis in Alzheimer's disease. Metallomics. 2011; 3:267–270. [PubMed: 21298161]

Castilla J, Saa P, Hetz C, Soto C. In vitro generation of infectious scrapie prions. Cell. 2005; 121:195–206. [PubMed: 15851027]

Caughey B, Baron GS, Chesebro B, Jeffrey M. Getting a grip on prions: oligomers, amyloids, and pathological membrane interactions. Annu Rev Biochem. 2009; 78:177–204. [PubMed: 19231987]

Chesebro B, Trifilo M, Race R, Meade-White K, Teng C, LaCasse R, Raymond L, Favara C, Baron G, Priola S, Caughey B, Masliah E, Oldstone M. Anchorless prion protein results in infectious amyloid disease without clinical scrapie. Science. 2005; 308:1435–1439. [PubMed: 15933194]

Choi CJ, Kanthasamy A, Anantharam V, Kanthasamy AG. Interaction of metals with prion protein: possible role of divalent cations in the pathogenesis of prion diseases. Neurotoxicology. 2006; 27:777–787. (2006). [PubMed: 16860868]

Choi CJ, Anantharam V, Saetveit NJ, Houk RS, Kanthasamy A, Kanthasamy AG. Normal cellular prion protein protects against manganese-induced oxidative stress and apoptotic cell death. Toxicol Sci. 2007; 98:495–509. [PubMed: 17483122]

Choi CJ, Anantharam V, Martin DP, Nicholson EM, Richt JA, Kanthasamy A, Kanthasamy AG. Manganese Upregulates Cellular Prion Protein and Contributes to Altered Stabilization and Proteolysis: Relevance to Role of Metals in Pathogenesis of Prion Disease. Toxicol Sci. 2010; 115:535–546. [PubMed: 20176619]

Das D, Luo X, Singh A, Gu Y, Ghosh S, Mukhopadhyay CK, Chen SG, Sy MS, Kong Q, Singh N. Paradoxical role of prion protein aggregates in redox-iron induced toxicity. PLoS One. 2010; 5:e11420. [PubMed: 20625431]

Deleault NR, Harris BT, Rees JR, Supattapone S. Formation of native prions from minimal components in vitro. Proc Natl Acad Sci USA. 2007; 104:9741–9746. [PubMed: 17535913]

Duce JA, Tsatsanis A, Cater MA, James SA, Robb E, Wikhe K, Leong SL, Perez K, Johanssen T, Greenough MA, Cho HH, Galatis D, Moir RD, Masters CL, McLean C, Tanzi RE, Cappai R, Barnham KJ, Ciccotosto GD, Rogers JT, Bush AI. Iron-export ferroxidase activity of β-amyloid precursor protein is inhibited by zinc in Alzheimer's disease. Cell. 2010; 142:857–867. [PubMed: 20817278]

Fernaeus S, Land T. Increased iron-induced oxidative stress and toxicity in scrapie-infected neuroblastoma cells. Neurosci Lett. 2005; 382:133–136. [PubMed: 16095817]

Fernaeus S, Halldin J, Bedecs K, Land T. Changed iron regulation in scrapie-infected neuroblastoma cells. Brain Res Mol Brain Res. 2005; 133:266–273. [PubMed: 15710243]

Goodbrand IA, Ironside JW, Nicolson D, Bell JE. Prion protein accumulation in the spinal cords of patients with sporadic and growth hormone associated Creutzfeldt-Jakob disease. Neurosci Lett. 1995; 183:127–130. [PubMed: 7746471]

Harrison PM, Arosio P. The ferritins: molecular properties, iron storage function and cellular regulation. Biochim Biophys Acta. 1996; 1275:161–203. [PubMed: 8695634]

Heiseke A, Aguib Y, Schatzl HM. Autophagy, Prion Infection and their Mutual Interactions. Curr Issues Mol Biol. 2010; 12:87–97. [PubMed: 19767652]

Hesketh S, Sassoon J, Knight R, Brown DR. Elevated manganese levels in blood and CNS in human prion disease. Mol Cell Neurosci. 2008; 37:590–598. [PubMed: 18234506]

Hur K, Kim JI, Choi SI, Choi EK, Carp RI, Kim YS. The pathogenic mechanisms of prion diseases. Mech Ageing Dev. 2002; 123:1637–1647. [PubMed: 12470901]

Hwang D, Lee IY, Yoo H, Gehlenborg N, Cho JH, Petritis B, Baxter D, Pitstick R, Young R, Spicer D, Price ND, Hohmann JG, Dearmond SJ, Carlson GA, Hood LE. A systems approach to prion disease. Mol Syst Biol. 2009; 5:252. [PubMed: 19308092]

Irjala K, Suonpää J, Laurent B. Identification of CSF leakage by immunofixation. Arch Otolaryngol. 1979; 105:447–448. [PubMed: 380535]

Iwasaki Y, Yoshida M, Hashizume Y, Kitamoto T, Sobue G. Neuropathologic characteristics of spinal cord lesions in sporadic Creutzfeldt-Jakob disease. Acta Neuropathol. 2005; 110:490–500. [PubMed: 16175355]

Johnstone D, Milward EA. Molecular genetic approaches to understanding the roles and regulation of iron in brain health and disease. J Neurochem. 2010; 113:1387–1402. [PubMed: 20345752]

Kell D. A systems biologist ponders how disparate ideas can sometimes come together beautifully. Nature. 2009; 460:6.

Kell DB. Towards a unifying, systems biology understanding of large-scale cellular death and destruction caused by poorly liganded iron: Parkinson's, Huntington's, Alzheimer's, prions, bactericides, chemical toxicology and others as examples. Arch Toxicol. 2010; 84:825–889. [PubMed: 20967426]

Kim BH, Jun YC, Jin JK, Kim JI, Kim NH, Leibold EA, Connor JR, Choi EK, Carp RI, Kim YS. Alteration of iron regulatory proteins (IRP1 and IRP2) and ferritin in the brains of scrapie-infected mice. Neurosci Lett. 2007; 422:158–163. [PubMed: 17614197]

Koorts AM, Viljoen M. Ferritin and ferritin isoforms I: Structure-function relationships, synthesis, degradation and secretion. Arch Physiol Biochem. 2007; 113:30–54. [PubMed: 17522983]

Kontoghiorghes GJ, Chambers SA, Victor Hoffbrand AV. Comparative study of iron mobilization from haemosiderin, ferritin and iron(III) precipitates by chelators. Biochem. J. 1987; 241:87–92. [PubMed: 3566714]

Lee DW, Andersen JK. Iron elevations in the aging Parkinsonian brain: a consequence of impaired iron homeostasis? J Neurochem. 2010; 112:332–339. [PubMed: 20085612]

Madsen E, Gitlin JD. Copper and iron disorders of the brain. Annu Rev Neurosci. 2007; 30:317–337. [PubMed: 17367269]

Mallucci GR, White MD, Farmer M, Dickinson A, Khatun H, Powell AD, Brandner S, Jefferys JG, Collinge J. Targeting cellular prion protein reverses early cognitive deficits and neurophysiological dysfunction in prion-infected mice. Neuron. 2007; 53:325–335. [PubMed: 17270731]

Martin DP, Anantharam V, Jin H, Witte T, Houk R, Kanthasamy A, Kanthasamy AG. Infectious prion protein alters manganese transport and neurotoxicity in a cell culture model of prion disease. Neurotoxicology. 2011

Meurman OH, Irjala K, Suonpää J, Laurent B. A new method for the identification of cerebrospinal fluid leakage. Acta Otolaryngol. 1979; 87:366–369. [PubMed: 443017]

Miller MB, Supattapone S. Superparamagnetic nanoparticle capture of prions for amplification. J Virol. 2011; 85:2813–2817. [PubMed: 21228242]

Molina-Holgado F, Hider RC, Gaeta A, Williams R, Francis P. Metals ions and neurodegeneration. Biometals. 2007; 20:639–654. [PubMed: 17294125]

Moore RA, Timmes A, Wilmarth PA, Priola SA. Comparative profiling of highly enriched 22L and Chandler mouse scrapie prion protein preparations. Proteomics. 2010; 10:2858–2869. [PubMed: 20518029]

Petersen RB, Siedlak SL, Lee HG, Kim YS, Nunomura A, Tagliavini F, Ghetti B, Cras P, Moreira PI, Castellani RJ, Guentchev M, Budka H, Ironside JW, Gambetti P, Smith MA, Perry G. Redox metals and oxidative abnormalities in human prion diseases. Acta Neuropathol (Berl). 2005; 110:232–238. [PubMed: 16096758]

Prusiner SB. Prions. Proc Natl Acad Sci USA. 1998; 95:13363–13383. [PubMed: 9811807]

Quintana C, Gutiérrez L. Could a dysfunction of ferritin be a determinant factor in the aetiology of some neurodegenerative diseases? Biochim Biophys Acta. 2010; 1800:770–782. [PubMed: 20447447]

Radford HE, Mallucci GR. The role of GPI-anchored PrP C in mediating the neurotoxic effect of scrapie prions in neurons. Curr Issues Mol Biol. 2010; 12:119–127. [PubMed: 19767655]

Rebouche CJ, Wilcox CL, Widness JA. Microanalysis of non-heme iron in animal tissues. J Biochem Biophys Methods. 2004; 58:239–251. [PubMed: 15026210]

Resenberger UK, Winklhofer KF, Tatzelt J. Neuroprotective and neurotoxic signaling by the prion protein. Top Curr Chem. 2011; 305:101–119. [PubMed: 21598098]

Rouault TA, Cooperman S. Brain iron metabolism. Semin Pediatr Neurol. 2006; 13:142–148. [PubMed: 17101452]

Saunders GC, Horigan V, Tout AC, Windl O. Identification of a proteinase K resistant protein for use as an internal positive control marker in PrP Western blotting. Res Vet Sci. 2007; 83:157–164. [PubMed: 17336356]

Singh A, Isaac AO, Luo X, Mohan ML, Cohen ML, Chen F, Kong Q, Bartz J, Singh N. Abnormal brain iron homeostasis in human and animal prion disorders. PLoS Pathog. 2009a; 5:e1000336. [PubMed: 19283067]

Singh A, Mohan ML, Isaac AO, Luo X, Singh N. Prion protein modulates cellular iron metabolism: Implications for prion disease pathogenesis. PLoS ONE. 2009b; 4:e4468. [PubMed: 19212444]

Singh A, Kong Q, Luo X, Petersen RB, Meyerson H, Singh N. Prion protein knock-out mice show altered iron metabolism: A functional role for PrP in iron metabolism. Plos ONE. 2009c; 4:e6115. [PubMed: 19568430]

Singh N, Singh A, Das D, Mohan ML. Redox control of prion and disease pathogenesis. Antioxid Redox Signal. 2010; 12:1271–1294. [PubMed: 19803746]

Singh A, Beveridge A, Gambetti P, Singh N. CSF transferrin is down-regulated in sCJD: a potential pre-mortem diagnostic test for prion disorders. PloS ONE. 2011; 6:e16804. [PubMed: 21408069]

Smith MA, Zhu X, Tabaton M, Liu G, McKeel DW Jr, Cohen ML, Wang X, Siedlak SL, Dwyer BE, Hayashi T, Nakamura M, Nunomura A, Perry G. Increased iron and free radical generation in preclinical Alzheimer disease and mild cognitive impairment. J Alzheimers Dis. 2010; 19:363–372. [PubMed: 20061651]

Soto C, Satani N. The intricate mechanisms of neurodegeneration in prion diseases. Trends Mol Med. 2010; 17:14–24.

Wang F, Wang X, Yuan CG, Ma J. Generating a prion with bacterially expressed recombinant prion protein. Science. 2010; 327:1132–1135. [PubMed: 20110469]

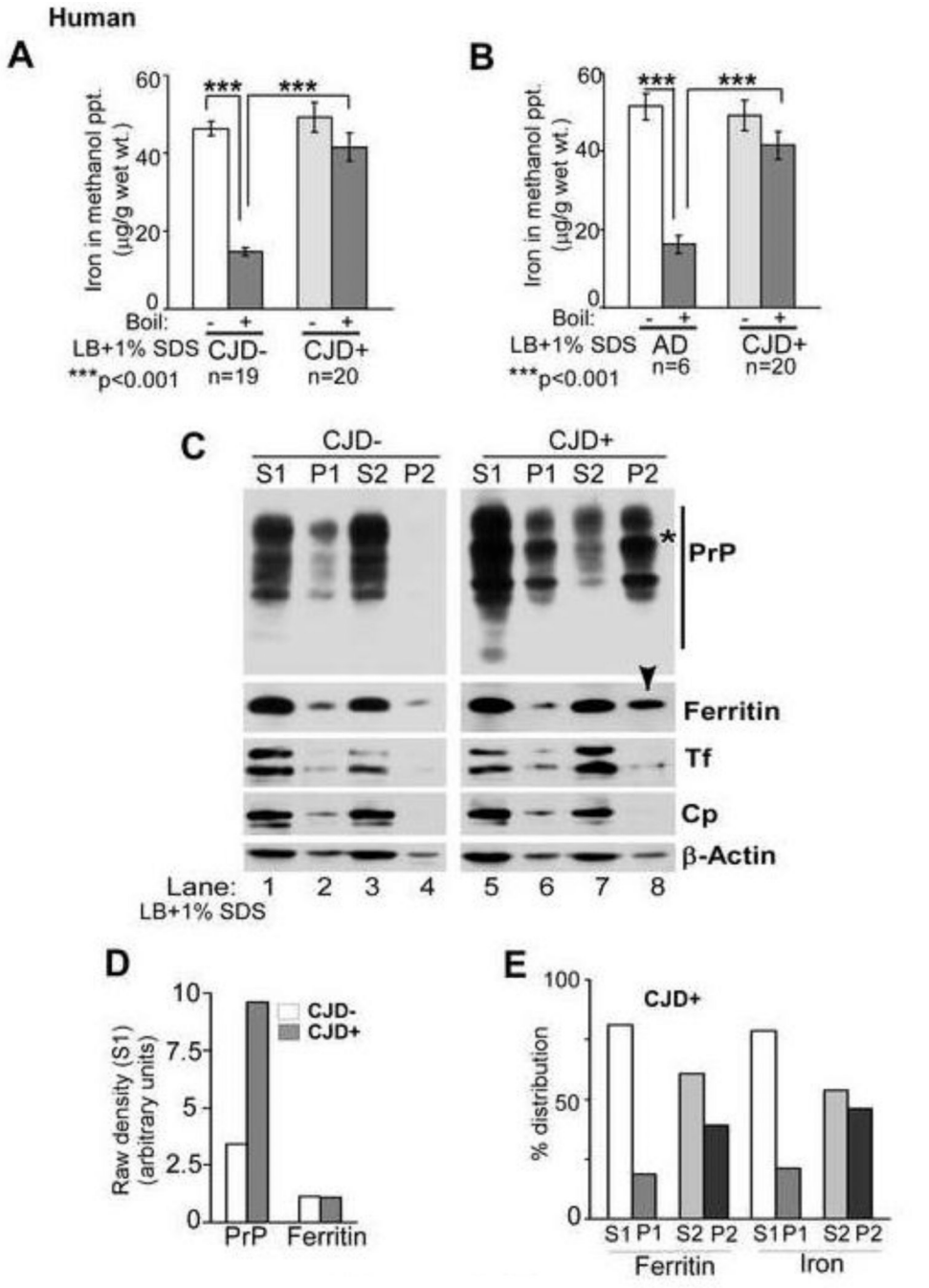

Figure 1. sCJD brain homogenates contain heat and SDS-stable pool of iron

(A) Methanol precipitated proteins from CJD− brain homogenates contain significantly less iron after boiling in the presence of SDS relative to unboiled samples. In contrast, precipitated proteins from CJD+ samples show minimal loss of associated iron after boiling. n=19 for CJD−, 20 for CJD+. ***p<.001. **(B)** Similar loss of protein associated iron is noted in AD samples after boiling with SDS, but not in CJD+ samples. n=6 for AD, 20 for CJD+. ***p<.001. **(C)** Differential centrifugation in the presence of SDS shows relatively more PrP^{Sc} relative to PrP^{C} in the low speed detergent soluble fraction (Figure 1 C, lanes 1 vs. 5), and partitioning of almost all PrP^{C} from CJD− samples in the high speed detergent soluble S2 fraction (lanes 3 & 4). In contrast, majority of PrP^{Sc} from CJD+ samples partitions in the

high speed detergent insoluble P2 fraction (lanes 7 & 8). Majority of Tf and Cp from both CJD− and CJD+ samples is detergent soluble and partitions in the high speed S2 fraction (lanes 3 & 7). Ferritin from CJD− samples partitions mainly in the S2 fraction, but a significant amount moves to the P2 fraction in CJD+ samples (lanes 3 & 4 vs. 7 & 8). β-actin shows similar intensity in S1 and S2 fractions of CJD− and CJD+ samples, indicating equal protein loading (lanes 1, 3, 5, & 7). (Representative data from 3 separate experiments is shown). **(D)** Quantification by densitometry after normalization with actin shows significantly more PrP in the S1 fraction of CJD+ relative to CJD− cases as expected, and insignificant difference in ferritin levels. **(E)** Percent distribution of protein associated iron in different fractions of CJD+ samples shows correspondence to ferritin levels.

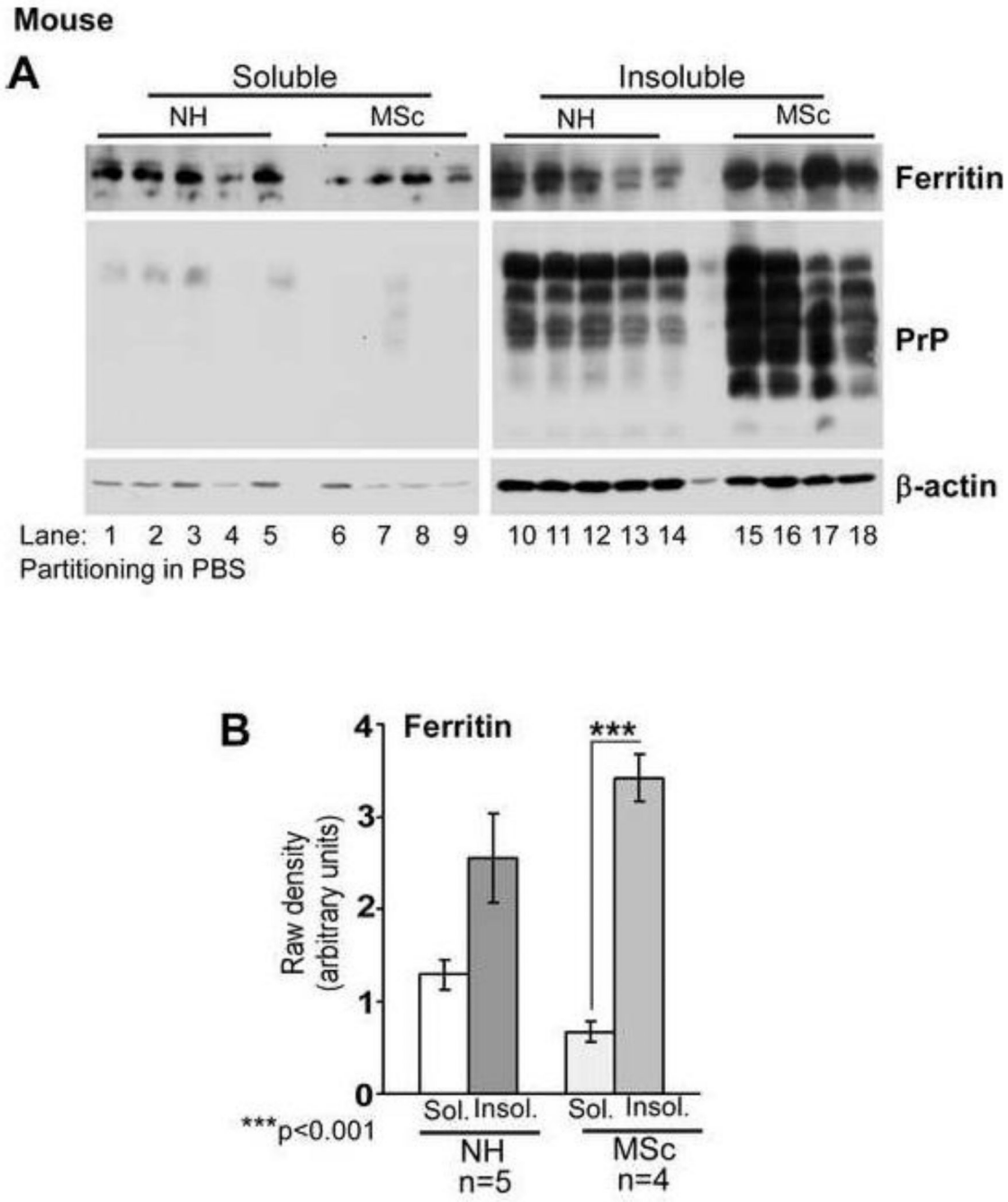

Figure 2. Ferritin in prion disease affected brains is denatured

(A) Fractionation in PBS reveals significantly more ferritin in the insoluble fraction of MSc samples relative to NH controls. PrP from both NH and MSc samples partitions in the insoluble fraction as expected. Actin mainly partitions in the insoluble fraction under these conditions. **(B)** Quantification by densitometry after normalization with actin reveals insignificant difference between soluble and insoluble fractions of ferritin from NH samples, while a significant amount of ferritin from MSc samples partitions in the insoluble fraction. n=5 for NH and 4 for MSc. ***p<.001.

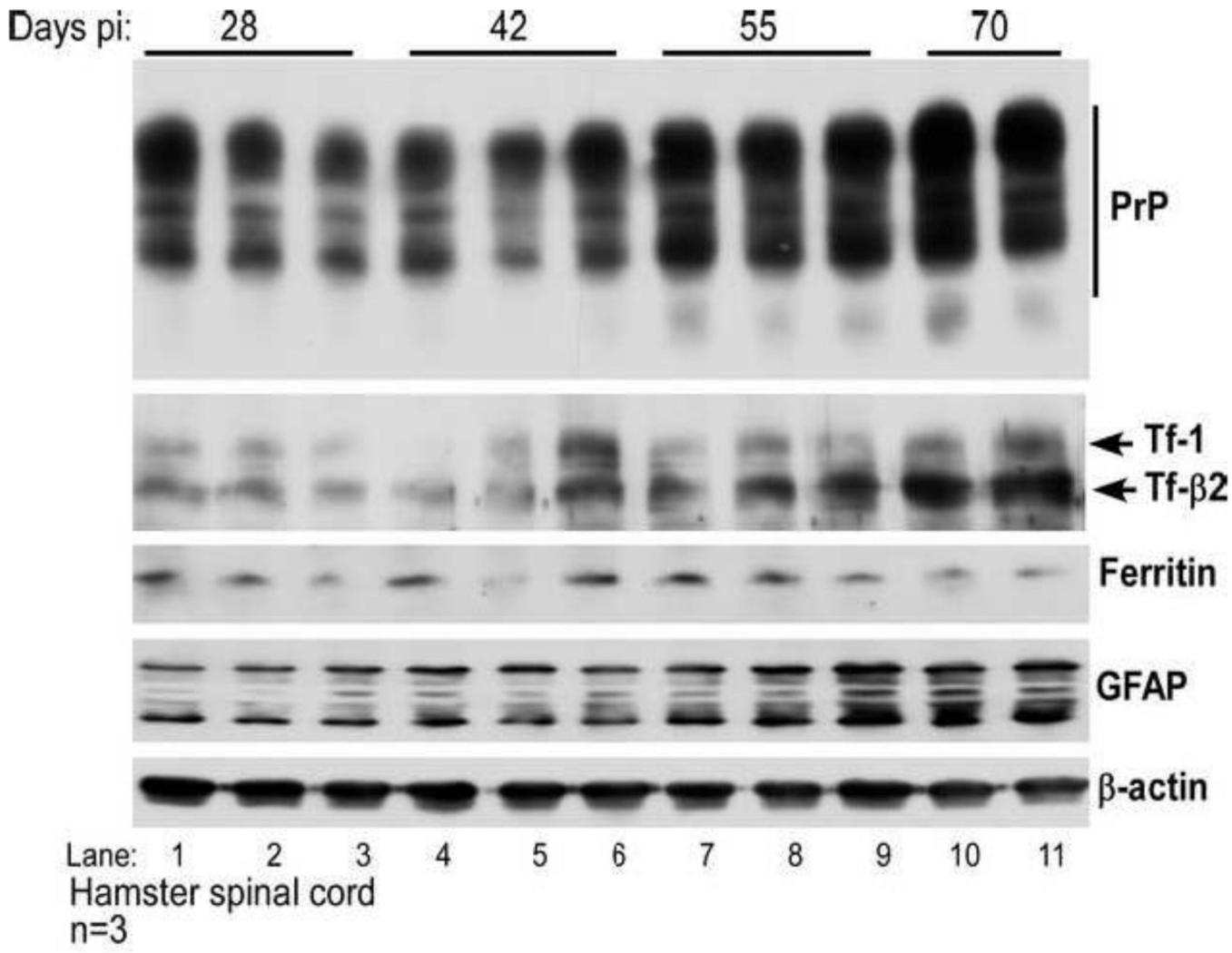

Figure 3. PrP and Tf increase with scrapie progression

Lumbar spinal cord tissue of scrapie inoculated hamsters was harvested at 28, 42, 55, and 70 days pi and subjected to Western blotting. Probing for PrP, Tf, and GFAP shows increase in expression with disease progression while ferritin shows minimal change despite significant astrogliosis (lanes 1–11). Re-probing for β-actin provides a control for protein loading.

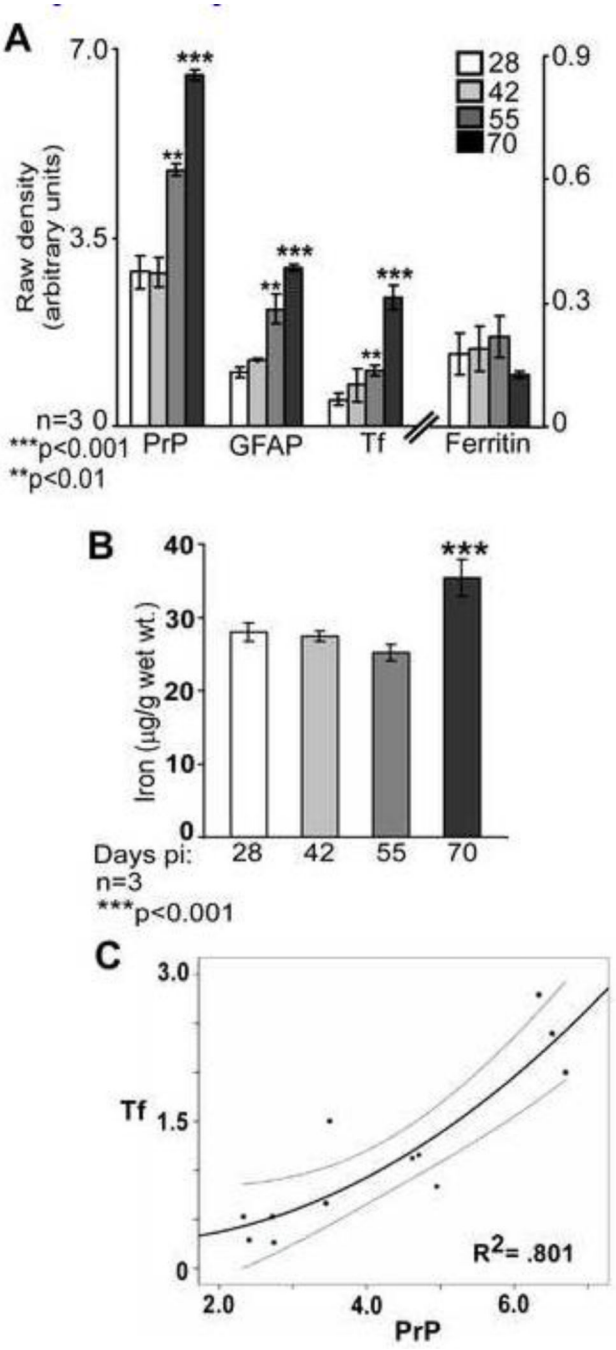

Figure 4. PrP and Tf show a direct correlation during disease progression

(A) Quantification by densitometry following normalization with actin shows a significant increase in PrP, GFAP, and Tf at 55 and 70 days pi relative to the 28 day sample. Ferritin levels do not show a significant change during disease progression. n=3. ***p*<0.01, ****p*<0.001. **(B)** Estimation of iron shows a significant increase at 70 days pi. n=3. ****p*<0.001. **(C)** Linear regression of Tf and PrP shows a significant correlation during disease progression. R^2=.801. n=3.

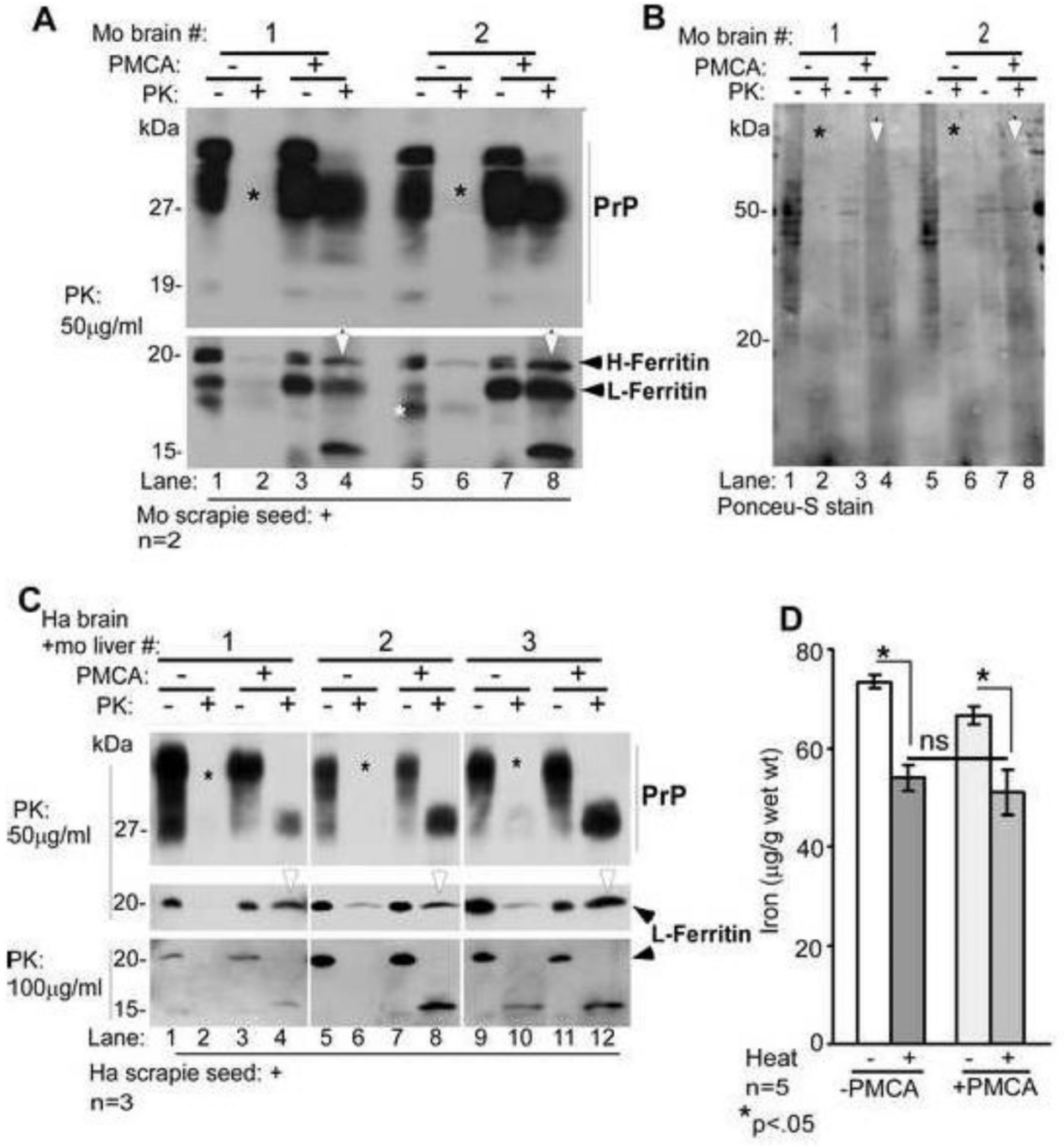

Figure 5. Amplification of PrP^{Sc} *in vitro* does not increase the heat stable pool of iron

(A) Normal mouse brain homogenate seeded with mouse scrapie was either set aside (−PMCA) or subjected to PMCA (+PMCA). Samples were treated with buffer (−PK) or PK (+PK) and subjected to Western blotting. Probing for PrP reveals the expected glycoforms in −PK samples (lanes 1, 3, 5, & 7). Treatment with PK causes complete degradation of PrP in −PMCA samples (lanes 2, & 6, *), and typical PK-resistant C-terminal fragments of PrP^{Sc} in +PMCA samples (lanes 4 & 8). Re-probing for ferritin shows similar pattern as PrP. Both isoforms of ferritin (H- and L-chain) are detected in −PK samples (lanes 1, 3, 5, & 7). PK treatment degrades both isoforms of ferritin in −PMCA samples (lanes 2 & 6), while +PMCA samples resist PK and show a faster migrating 15kDa form (lanes 4 & 8). A

representative blot from five separate experiments is shown. **(B)** Visualization of transferred proteins by Ponceu-S stain shows an overall decrease in +PMCA samples (lanes 3, 4, 7, & 8, *), and increased PK resistance of several proteins in PMCA samples (lanes 4 & 8 vs. 2 & 6, white arrow-heads). **(C)** Similar evaluation of hamster brain and mouse liver homogenates seeded with hamster scrapie reveals PK-resistant PrP^{Sc} and ferritin in +PMCA samples (lanes 4, 8, & 12), not in −PMCA samples (lanes 2, 6, & 10). Increase in the concentration of PK reveals a faster migrating PK resistant fragment of ferritin (lanes 4, 8, & 12). **(D)** Iron associated with methanol precipitated protein pellet from −PMCA and +PMCA samples decreases significantly after boiling as expected. However, there is no difference in the iron content of boiled −PMCA and +PMCA samples despite successful amplification of PrP^{Sc}. A and C are representative blots of 3 different experiments. n=5. *$p<0.05$.

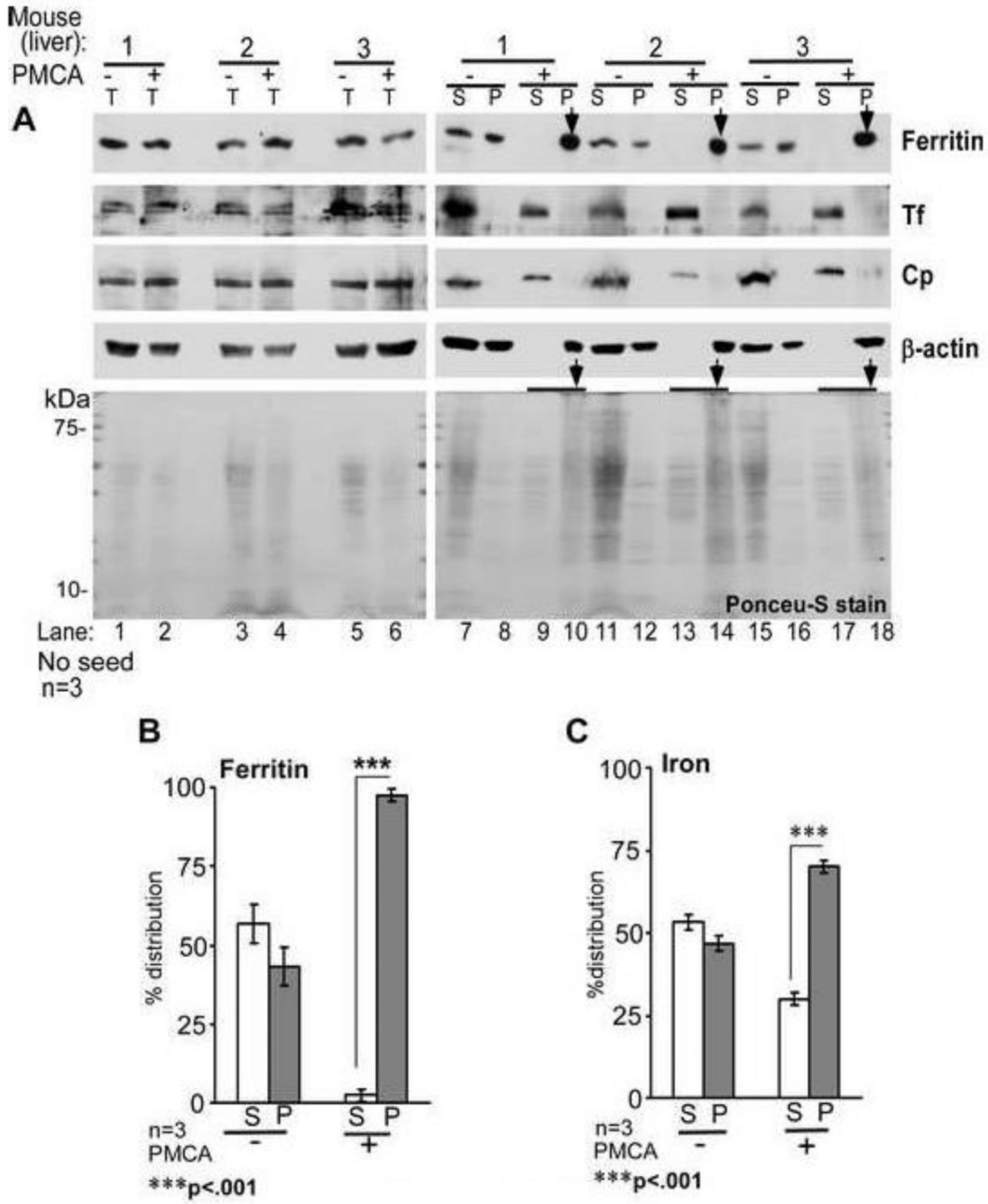

Figure 6. PMCA reaction induces aggregation of ferritin in liver homogenates

(A) Normal mouse liver homogenates subjected to PMCA (+PMCA) or not (−PMCA) were centrifuged to separate detergent soluble (S) and insoluble (P) fractions, and analyzed by Western blotting. Probing of total (T) samples before centrifugation reveals equal distribution of ferritin in −PMCA and +PMCA samples (lanes 1–6). Following centrifugation, ferritin partitions equally between S and P fractions in −PMCA samples (lanes 7, 8, 11, 12, 15, & 16), but shifts almost completely to the P fraction following PMCA (lanes 10, 14, & 18, *). Unlike ferritin, Tf and Cp remain in the S fraction even after PMCA (lanes 7, 9, 11, 13, 15, & 17). Surprisingly, β-actin also aggregates by PMCA (lanes 10, 14, & 18). Ponceu-S staining of all proteins reveals slight degradation by PMCA (lanes 2, 4, &

6) and PK resistance of several proteins in the P fraction (lanes 10, 14, & 18). A representative blot of 3 different experiments is shown. **(B)** Percent distribution of ferritin shows 97.5% in the P fraction following PMCA. Since β-actin aggregates by PMCA, lanes 1–6 were used as loading controls for lanes 7–18. n=3. ***p<.001. **(C)** Protein-associated iron shows similar distribution as ferritin. Non-correspondence of ferritin and iron in the S fraction of +PMCA samples is due to contribution from low molecular weight iron compounds and soluble iron rich proteins such as Tf. n=3. ***p<.001.